Instability Attenuation And Bifurcation Studies of A Non-Ideal Rotor Involving Time Delayed Feedback

Sovan Sundar Dasgupta (sovan@vit.ac.in)
VIT University https://orcid.org/0000-0003-1325-1792

Research Article

Keywords: Internal damping, Sommerfeld effect, Time delayed feedback, Bifurcations, Non-ideal system, Jump phenomena, AMB

Posted Date: November 16th, 2021

DOI: https://doi.org/10.21203/rs.3.rs-969838/v1

Version of Record: A version of this preprint was published at Nonlinear Dynamics on March 25th, 2022.
See the published version at https://doi.org/10.1007/s11071-022-07367-w.

Instability attenuation and bifurcation studies of a non-ideal rotor involving time delayed feedback

Sovan Sundar Dasgupta

School of Mechanical Engineering, VIT, Vellore, Tamil Nadu, India

E-mail: sovan@vit.ac.in

Abstract

In non-ideal vibratory system, the excitation is a nonlinear function of system response. The dynamic behavior of such system is often characterized by an energy source with limited power. The study of instability phenomena in non-ideal rotor driven through a non-ideal energy source is of considerable current interest. The non-ideal rotor system often gets destabilized on exceeding a critical input power near the resonance. This kind of instability is termed as Sommerfeld effect marked with nonlinear jump phenomena. This paper investigates the attenuation of nonlinear jump phenomena and numerical study of bifurcations of a non-ideal unbalanced rotor system with internal damping using time delayed feedback via active magnetic bearings. The results show that the time delay indeed plays a critical role on the suppression of the jump phenomena. Following, some new insights are also revealed through a numerical study of saddle node, Hopf and trans-critical bifurcations with time delay as a bifurcation parameter. The transient analysis confirms the results obtained analytically through the steady-state consideration.

Keywords Internal damping; Sommerfeld effect; Time delayed feedback; Bifurcations; Non-ideal system; Jump phenomena; AMB

1 Introduction

The control of instability of high-speed non-ideal rotor system has been considered a great challenge to many researchers in recent times. These rotors are coupled with an energy source with limited power (*i.e.,* DC motor, induction motor *etc*) which also gets affected by the response of the system contrary to its ideal counterpart in which the source is not influenced by the system response [1]. Mathematical modelling of such non-ideal systems involves an additional degree of freedom which describes the nonlinear interaction of the rotor system with the electric motor. The interaction between the motor and the rotor system is highly complex and nonlinear. During the coast up operation, close to the system resonance, the rotor speed suddenly jumps to a very high value and the corresponding amplitude simultaneously jumps to a very low value on exceeding a critical power input of the motor. A similar kind of jump in the reverse manner is also observed during the coast down operation wherein the spin speed jumps to a very low value and the corresponding amplitude jumps to a very high value. This jump phenomena marked with a curve of discontinuity is observed in the frequency response which reveals that certain spin speeds could not be achieved during the steady-state when the input power exceeds a critical value. This kind of jump phenomena is well-known as Sommerfeld effect [2] which often destabilizes the system near the resonance. The non-conservative circulatory forces due to intrinsic material damping also causes the system unstable beyond a certain threshold spin speed which is referred to as a second kind of Sommerfeld effect in rotor dynamics literature [3].

A few studies are reported so far dealing with the attenuation of instability for non-ideal systems. A tuned liquid damper is proposed by Felix et al., [4] as a passive control strategy which successfully attenuated the instability of a structural frame excited through a non-ideal excitation. A kind of friction model is employed to mitigate the Sommerfeld effect of a non-ideal structure using a vibration absorber [5]. Semi-active control technique is also employed to study the Sommerfeld effect mitigation such as using MR damper on a non-ideal vibratory system powered through a DC motor is reported by Castao et.al., [6]. Another important work on the suppression of non-linear jump phenomena using a magnetorheological damper is reported in [7]. In 2018, Balthazar and his co-authors proposed an experimental technique using shape memory element to mitigate the jump phenomena exhibited by a non-ideal cantilever [8]. In the recent past, a novel approach [9] based on fractional order external damping is employed to study the attenuation of the jump phenomena of a non-ideal internally damped shaft-disk system. Subsequently, a semi-active control scheme through a switched stiffness device was also proposed by the same authors [10].

Active Magnetic bearing (AMB) has many advantages over its passive counterpart such as non-contacting nature of suspension over the convention fluid film and anti-friction bearings, elimination of lubricant, very low friction, no wear, high rotor speed and high load carrying capacity at extreme conditions such as very high or very low temperature and vacuum. Many scientific articles dealing with control of rotating machinery *via* AMB system have been published [11–20]. But AMB based active control strategy dealing with suppression of the Sommerfeld effect in non-ideal internally damped rotor system was not reported before 2019. In 2019, Jha and Dasgupta proposed an active control scheme based on a linearized model of AMB system to attenuate the Sommerfeld effect in a non-ideal rotor disk with material damping successfully [21].

It is well-known that the time delay often destabilizes the system. Thus, the analysis of the dynamic behaviour of AMB with time delay is extremely important. The source of the intrinsic time delay is due to the hardware of the digitally controlled AMB system which comprises digital signal processor (DSP), analog-to-digital (A/D) and digital-to-analog (D/A) converters, memory, filters, interfacing components *etc*. Usually, a multiplexer topology is employed for multiple A/D conversion channels for sampling. Improper synchronization of A/D converters with sample and hold circuit, delay in A/D and D/A conversion, computational dead time may have adverse effect on the phase margin of the system leading to instability. A few works discussed the problem of the time-delays in AMB-system [20, 22–24]. Influence of time delay is reported in [22] to study the stability of a Jeffcott rotor-AMB system based on Hopf bifurcations. In a similar kind of study, it has been shown that on exceeding a critical time delay, instability occurs in a rotor system coupled with AMB [23]. Following, occurrence of period-doubling bifurcations is investigated in a system with time-delayed magnetic levitation marked with soft spring characteristics [24]. A study on vibration suppression of a time-delayed AMB system subjected to multi-parametric excitation is reported in [20]. This study also reveals that the efficacy of the controller may be enhanced if the time delay is kept within a stable range. Eissa et al. [25] studied the effectiveness of a time-delayed PD controller to attenuate the instability of a nonlinear system coupled with a magnetic bearing. Balthazar et al [26], studied the Hopf bifurcation on a centrifugal vibrator actuated by a non-ideal motor. However, influence of time delay in attenuating the Sommerfeld effect of non-ideal eccentric rotor system with internal damping is not yet reported so far. The bifurcation studies of such non-ideal systems are also not available in literature.

This paper aims to present the influence of intrinsic time delay in attenuating the nonlinear jumps of a non-ideal rotor-AMB system driven through a brushed DC motor. Moreover, it also reveals the complex dynamics of this non-ideal system through different bifurcation studies (such as saddle node, Hopf and trans-critical) with the help of root-loci plots. The rest of the paper organised as follows. Section 2 gives the mathematical modelling of the proposed system with time delay. Section 3 discusses the influence of time delay in attenuating the Sommerfeld effect. Following a transient analysis is also performed which confirms the analytical results given in Section 3. Numerical studies of bifurcations through a set of root-locus plots are presented in Section 4 which reveal the complex dynamics of instability influenced by the time delay based on certain conditions. Section 5 gives the conclusions and future work. The steady-state amplitude frequency responses close to the system resonance are obtained for several time delays. Following, a transient analysis is found to be in good agreement with the steady-state results.

2 Model description and equations of motion

A typical internally damped non-ideal eccentric rotor-AMB system with time delay driven through a brushed DC motor is considered for the present work as shown in the Fig. 1. The system equations of the proposed rotor-disk model required to perform analytical and transient analysis are presented in the following subsections.

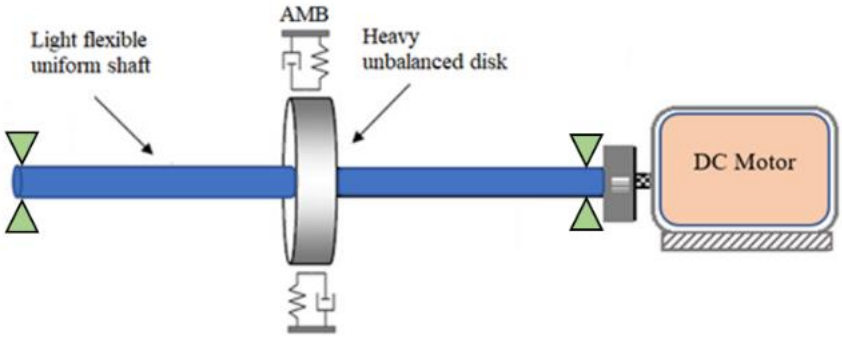

Fig. 1 Schematic of a non-ideal rotor-AMB system with time delay

2.1 Equations of motion

A flexible internally damped shaft driven through a brushed DC motor supported by a pair of identical rigid bearings is shown in the Fig. 1. A small disk is mounted with small eccentricity at the mid-span of the shaft. No gyroscopic term is involved as the disk is centrally mounted. Additionally, two identical AMBs with a small time delay (τ) are employed as shown in Fig. 1. The proposed model offers one more degree of freedom (DOF) to describe the nonlinear complex interaction between the system and non-ideal DC motor. Using the Lagrange-differential equations, the generalized vector differential equation may be obtained as follows:

$$\mathbf{M}\ddot{\mathbf{q}} + \mathbf{D}\dot{\mathbf{q}} + (\mathbf{K} + \mathbf{H})\mathbf{q} = \mathbf{F}(t) + \mathbf{F}_c(t-\tau). \tag{1}$$

Eq. (1) represents a delay differential equation (DDE) [27] which is typical representative of infinite-dimensional system [27] as time delay (τ) is exclusively present in the RHS of the Eq. (1). The non-linear system with the time-delays has been an active topic of research over the past decades [19, 20, 28, 29]. In the present system, the main sources of instability are due to non-conservative internal damping and time delay induced source loading term. The nonlinear interaction between the DC motor and the system may be represented by the following equation:

$$I\ddot{\theta} + R_r\dot{\theta} = T_m - T_L \tag{2}$$

where

$$\mathbf{M} = \begin{bmatrix} m & 0 \\ 0 & m \end{bmatrix},\ \mathbf{D} = \begin{bmatrix} R_e + R_i & 0 \\ 0 & R_e + R_i \end{bmatrix},\ \mathbf{K} = \begin{bmatrix} K & 0 \\ 0 & K \end{bmatrix},\ \mathbf{H} = R_i\dot{\theta}\begin{bmatrix} 0 & 1 \\ -1 & 0 \end{bmatrix},\ \mathbf{F}(t) = \begin{Bmatrix} me\dot{\theta}^2\cos(\theta+\varphi) \\ me\dot{\theta}^2\sin(\theta+\varphi) \end{Bmatrix},\ \mathbf{q} = \begin{Bmatrix} x \\ y \end{Bmatrix},$$

$\mathbf{M}, \mathbf{D}$ and $\mathbf{K}$ are symmetric and positive definite diagonal matrices, $\mathbf{H}$ is an anti-symmetric circulatory matrix [30] $(i.e.,\ \mathbf{H} = -\mathbf{H}^{\mathbf{T}})$ which may destabilize the system involving material damping (R_i) [31], $\mathbf{q}$ is a 2×1 column vector of generalized coordinates. The material damping in rotor dynamics plays a key role in determining the stability of the system. It is considered to be a function of past history of loading, strain rate and temperature of the system. Owing to the presence of R_i, the follower types circulatory forces (F_{CH}) appear in the source loading (*see* Eq. 4) is non-conservative in nature as $\nabla \times F_{CH} \neq 0$, causes self-excited vibration, θ represents the angular rotation of the eccentric disk. On the right-hand side of Eq. (1), the second term, $\mathbf{F}_c(t-\tau)$ represents control force provided by the AMB actuator with time delay (τ). In the RHS of Eq. (2), T_m and T_L represent the torque supplied by the DC motor, and the nonlinear source loading torque respectively. The parameters used in Eq. (1) & Eq. (2) are presented in Table 1.

Table 1

Symbol	Name of the disk and motor parameters
m	mass of the centrally mounted disk
I	mass moment of inertia of the shaft-rotor system about the axis of spin
R_e	external damping referred to the disk centre
R_i	internal or material damping referred to the disk centre
R_r	damping offered by the bearings and medium to the system
R_m	armature resistance of the DC motor
V_s	supply voltage
μ_m	DC motor characteristic constant
e	constant small eccentricity in the disk
φ	phase corresponding to initial position of mass centre of the disk

2.2 AMB Model with time delay

AMB system suspends rotor through electromagnetic force, thereby eliminating physical contact with the bearing. A schematic diagram of AMB system with time delay is shown in Fig. 2. A Hall-effect based proximity sensor senses the rotor displacement and sends the signal as a negative-feedback to the controller. The controller, based on a control law, generates the control current which then passes through a time delay block to incorporate a delay. Then the time delayed signal gets amplified by the power amplifier. Following, control force is built up in the electromagnetic actuator which applies on the rotor shaft.

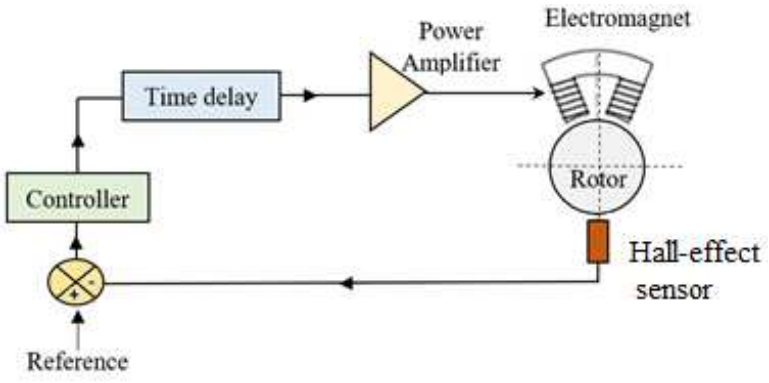

Fig. 2 Schematic of an AMB system with time delay

In the present study, the control currents given by the AMB system along the x and y direction according to Proportional-Derivative (PD) control scheme are expressed as: $i_{x-\tau} = -K_p K_a \left(x(t-\tau) + K_d \dot{x}(t-\tau) \right)$ and $i_{y-\tau} = -K_p K_a \left(y(t-\tau) + K_d \dot{y}(t-\tau) \right)$. Using the control currents $\left(i_{x-\tau} \ \& \ i_{y-\tau} \right)$, the time delayed linearized control force $\left(\mathbf{F_c}(t-\tau) \right)$ may be expressed as:

$$\mathbf{F_c}(t-\tau) = \begin{bmatrix} f_x^{AMB}(t-\tau) \\ f_y^{AMB}(t-\tau) \end{bmatrix} = -\begin{bmatrix} K_{AMB} & 0 \\ 0 & K_{AMB} \end{bmatrix} \begin{Bmatrix} x(t-\tau) \\ y(t-\tau) \end{Bmatrix} - \begin{bmatrix} C_{AMB} & 0 \\ 0 & C_{AMB} \end{bmatrix} \begin{Bmatrix} \dot{x}(t-\tau) \\ \dot{y}(t-\tau) \end{Bmatrix} \tag{3}$$

where $K_{AMB} = -K_u + K_i K_a K_p K_s$ and $C_{AMB} = K_i K_a K_p K_s K_d$, $K_i = 4Ki_o / c^2$ and $K_u = 4Ki_0^2 / c^3$. The AMB parameters are given in Table 2. Details of the derivation is given in [30].

Table 2

Symbol	Name of the AMB parameters
K_s	sensor gain
K_a	gain of the power amplifier
K_p	proportional gain of the controller
K_d	derivative gain of the controller
i_0	bias current
c	radial clearance

Usually, the time delay present in the digitally controlled AMB actuators is finite [19]. Thus, the displacement and the velocity feedback terms given in Eq. (3) may be approximated as [32]:

$$\left.\begin{aligned} x(t-\tau) &\approx (x-\tau\dot{x}), \dot{x}(t-\tau) \approx (\dot{x}-\tau\ddot{x}) \\ y(t-\tau) &\approx (y-\tau\dot{y}), \dot{y}(t-\tau) \approx (\dot{y}-\tau\ddot{y}) \end{aligned}\right\} \tag{4}$$

Assumption of finite time delay justifies the reality of digitally controlled AMB system and in no way affects the accuracy of the analysis. Thus, the resulting system turns out to be finite dimensional. Making use of Eq. (4), Eq. (1) & (2) makes the Eq. (1) into a finite two-dimensional ODE as follows:

$$\mathbf{M}'\ddot{\mathbf{q}} + \mathbf{D}'\dot{\mathbf{q}} + (\mathbf{K}' + \mathbf{H})\mathbf{q} = \mathbf{F}(t) \tag{5}$$

where

$$\mathbf{M}' = \begin{bmatrix} \bar{M} & 0 \\ 0 & \bar{M} \end{bmatrix},\ \mathbf{D}' = \begin{bmatrix} \bar{C} & 0 \\ 0 & \bar{C} \end{bmatrix},\ \mathbf{K}' = \begin{bmatrix} \bar{K} & 0 \\ 0 & \bar{K} \end{bmatrix},\ \mathbf{H} = \begin{bmatrix} 0 & R_i\dot{\theta} \\ -R_i\dot{\theta} & 0 \end{bmatrix},\ \mathbf{F}(t) = \begin{Bmatrix} me\dot{\theta}^2\cos(\theta+\varphi) \\ me\dot{\theta}^2\sin(\theta+\varphi) \end{Bmatrix},\ \mathbf{q} = \begin{Bmatrix} x \\ y \end{Bmatrix}$$

and $\bar{M} = m - \tau C_{AMB}$, $\bar{C} = R_e + R_i + C_{AMB} - \tau K_{AMB}$, $\bar{K} = K + K_{AMB}$.

The RHS terms in Eq. (2) *i.e.,* the torque supplied (T_m) by the DC motor, and the nonlinear source loading torque (T_L) given in Eq. (2) may be further expressed as:

$$T_m = \mu_m\left(V_s - \mu_m\dot{\theta}\right)/R_m \tag{6}$$

$$T_L = R_i\left(x\dot{y} - \dot{x}y\right) + \left[\bar{C}\dot{x} + \bar{K}x\right]e\sin\theta - \left[\bar{C}\dot{y} + \bar{K}y\right]e\cos\theta \tag{7}$$

2.3 Stability condition of the steady-state response

Owing to the isotropic nature of external and internal damping, Eq. (3) admits a special orthogonal group with dimensions two (SO(2)) symmetry [33, 34]. Hence a self-symmetric solution under SO(2) may be expressed as $x = F_0\cos(\omega_r t + \beta)$ and $y = F_0\sin(\omega_r t + \beta)$. The steady-state synchronous whirl amplitude (F_0) may be expressed as:

$$F_0 = me\omega_r^2 / \left[\left((K + K_{AMB}) - \bar{M}\omega_r^2\right)^2 + C_d^2\omega_r^2\right]^{1/2} \tag{8}$$

where $C_d = \left(R_e - \tau K_{AMB} + C_{AMB}\right)$ and the phase angle, $\beta = \left(\tan^{-1}\left(y/x\right) - \omega_r t\right)$. Here, synchronous whirl amplitude is not influenced by the material damping as the speed of the non-ideal energy source (*i.e.,* DC motor) is assumed to be constant.

It is well-known that for a critical circulatory parameter $\left(i.e., \gamma_{crit} = \omega_r R_i, \gamma_{crit} > 0\right)$ [35] the energy supplied to system $\left(W_m\right)$ equals to the energy dissipated by the system $\left(W_d\right)$. Applying this condition on the previous equations [36], a polynomial of 5th order is obtained as follows:

$$\left(\bar{M}^2\left(\mu_m^2 + R_m R_r\right) + m^2 e^2 R_m \bar{C}\right)\omega_r^5 - \bar{M}^2 \mu_m V_s \omega_r^4 - \left(\mu_m^2 + R_m R_r\right)\left(2\bar{M}\bar{K} - C_d{}^2\right)\omega_r^3 + \mu_m V_s \left(2\bar{M}\bar{K} - C_d{}^2\right)\omega_r^2$$
$$+\bar{K}^2\left(\mu_m^2 + R_m R_r\right)\omega_r - \bar{K}^2 \mu_m V_s = 0. \qquad (9)$$

It is obvious that not all the roots of the Eq. (9) give stable solutions. Using the approach given in [37] which states that a stable energy state exists if and only if $\left(W_m - W_d\right)$ happens to be a decreasing function for a critical value of ω_r say ω_{rc} . This criterion ensures possible existence of a locally minimum energy state and every root satisfying the above criterion must lie on the stable branch. Moreover, the term given in Eq. (9) $\left(2\bar{M}\bar{K} - C_d{}^2\right) > 0$ implies the number of positive real roots may be three or one according to the Descarte's sign rule. Thus, the existence of multiple roots confirms the presence of the Sommerfeld effect marked with nonlinear jumps [38, 39].

3 Influence of time delay and bias current on attenuation of the Sommerfeld effect

Using the system parameters [21] (*see* Table 3) and making use of Eq. (9) along with the minimum energy state criterion as mentioned above, the following numerical simulations are carried out.

Table 3

System Parameter	Value	System Parameter	Value
m	2 kg	R_e	150 Ns/m
K	8×10^4 N/m	R_i	50 Ns/m
e	0.001 m	R_r	2×10^{-5} Nm s /rad
R_m	40 Ω	μ_m	0.1 Nm/A
I	0.004 kg.m^2	ω_n	200 rad/sec.

The result presented in Fig. 3 is in good agreement with [21] in which during coast up phase, the non-dimensional whirl amplitude $\left(\beta = B\omega_n^2 / g\right)$ jumps from a higher value ('*b*') to a lower value ('*d*') nearer to resonance, upon exceeding a critical input power while the non-dimensional rotor spin speed $\left(\omega_r^* = \omega_r / \omega_n\right)$ jumps simultaneously from a lower ('*b*') to higher value ('*d*') with no AMB and no time delay *i.e.,* $i_a = 0 \quad \tau = 0.$ Similarly, during coast down, the amplitude jumps to a higher value ('*a*') and from '*c*' whereas the rotor speed goes to a lower value at ('*a*').

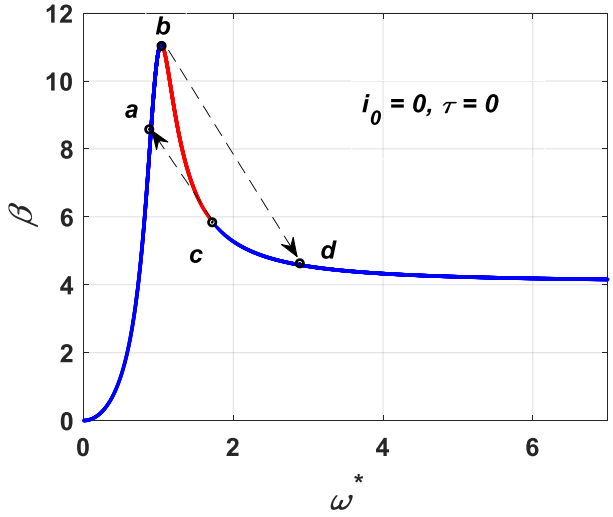

Fig. 3 Steady-state amplitude frequency response without AMB

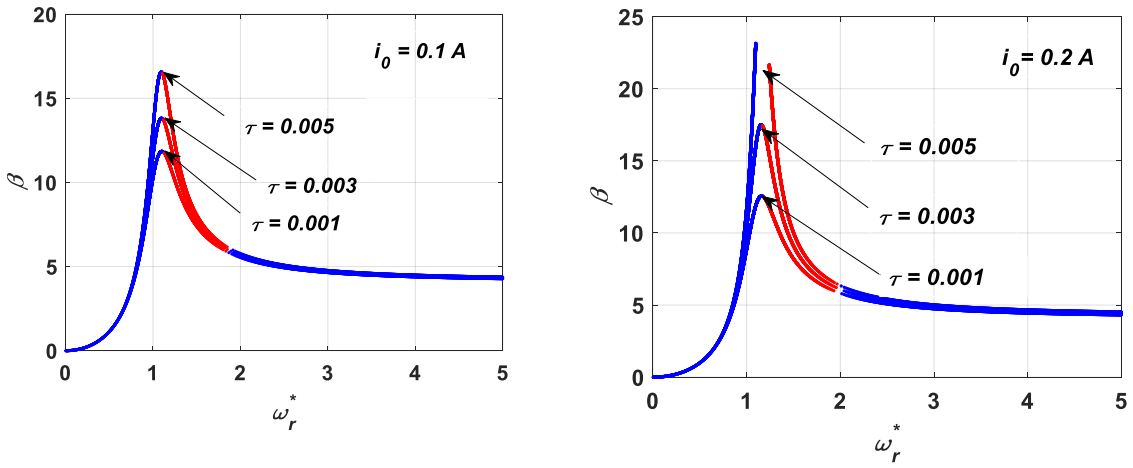

(a) **(b)**

Fig. 4 (a) & (b) Steady-state amplitude frequency response with fixed bias current and various time delays

Fig. 4 (a) and Fig. 4 (b) illustrate the attenuation of the Sommerfeld effect as time delay decreases for some fixed bias current. The similar phenomena are observed when the non-dimensional spin speed amplitude and *versus* non-dimensional supply voltage as shown in Fig. 5 and Fig. 6 respectively for several time delays with a given bias current. The transient analysis shown in Fig. 8 (a) confirms the steady results illustrated in Fig. 4 (a) & (b).

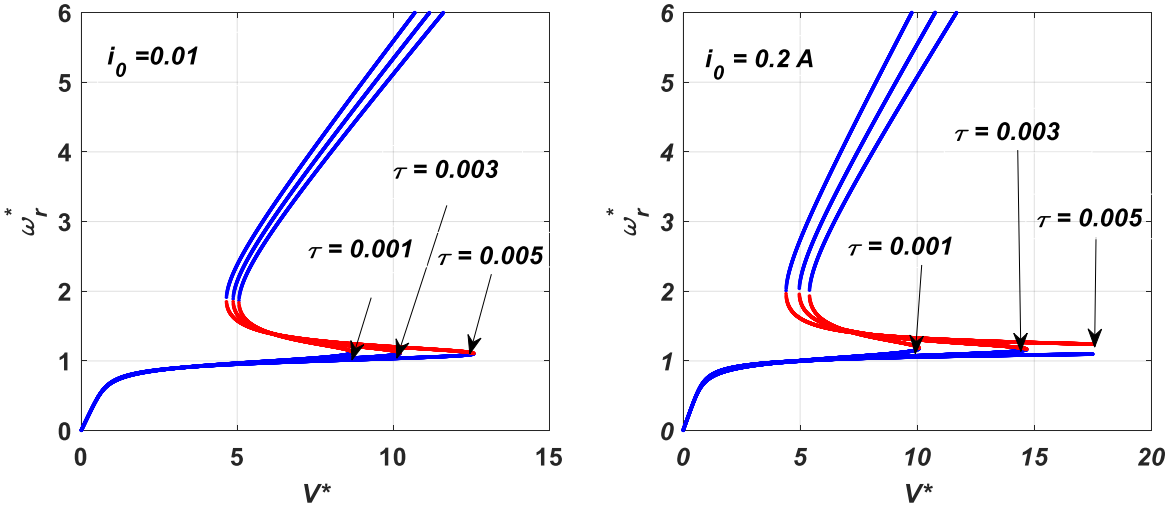

Fig. 5 (a) & (b) Steady-state spin speed variation with supply voltage for fixed bias current and various time delays

On the other hand, if the time delay is fixed, the Sommerfeld effect is found to be attenuated as the bias current decreases (see Fig. 7 (a) & (b)) which is contrary to the results reported in [21] wherein the Sommerfeld effect is found to be reduced gradually as the bias current increases for the same non-ideal system without time delay. This result suggests that the AMB system with time delay is not only more realistic but also advantageous as it requires very small current to suppress the Sommerfeld effect. The same result is also true for the rotor speed and amplitude *versus* supply voltage graphs. The transient analysis illustrated in Fig. 8 (b) confirms the above result. The transient study shown in Fig. 9 is found to be in good agreement with the steady-state result.

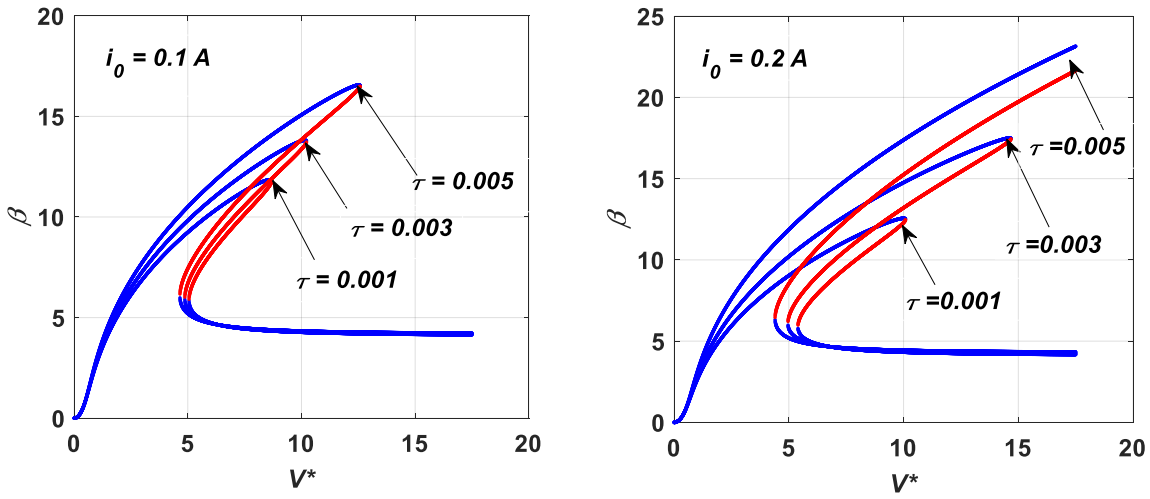

Fig. 6(a) & (b) Steady-state amplitude variation with supply voltage for fixed bias current and various time delays

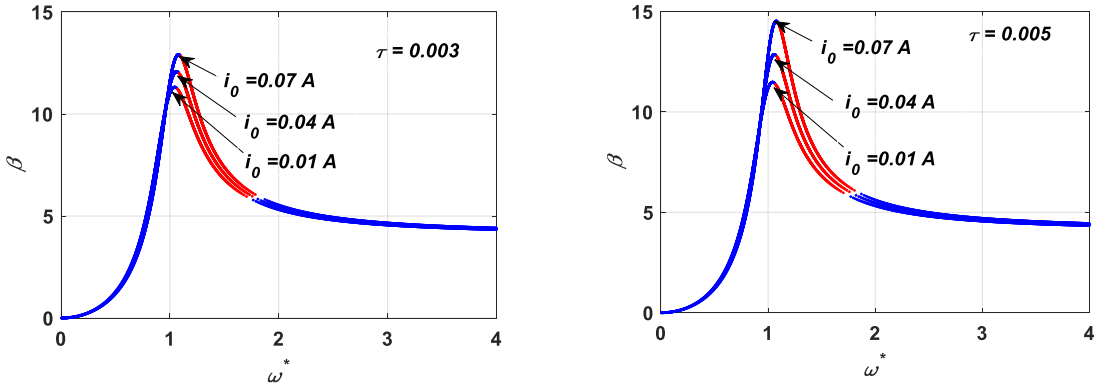

Fig. 7 (a) & (b) Steady-state amplitude variation with spin speed for fixed time delay and various bias currents

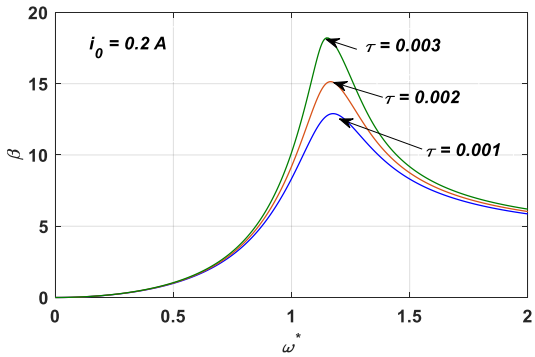

Fig. 8 (a) Sommerfeld effect attenuation for a fixed bias currents and various time delays

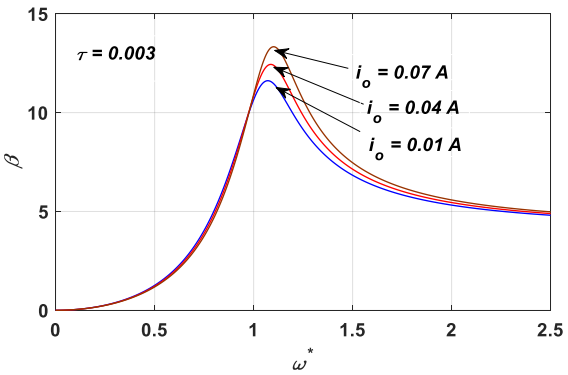

Fig. 8 (b) Sommerfeld effect attenuation for a fixed time delay and various bias currents

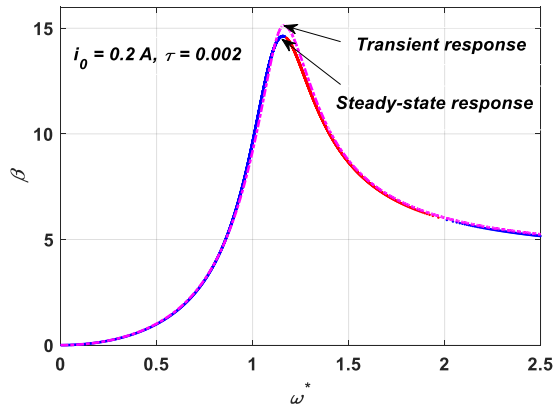

Fig. 9 A comparison between transient and steady-state response

4 Bifurcation analysis

The study of instability phenomena characterized with nonlinear jumps seems to be more realistic and convincing when time delay is considered. Delay induced bifurcation studies in a complex dynamical system reveal a couple of interesting facts. In the following sub- sections, numerical experimentations of saddle-node, Hopf and trans-critical bifurcations are carried out systematically with the help of root loci technique [40].

4.1 Root locus method

Using a fifth order polynomial of ω_r given in Eq. (9), one may write the following transfer function between a fictitious input and output pair as:

$$G(s)=\frac{N(s)}{D(s)}=\frac{N_4 s^4+N_2 s^2+N_0}{D_5 s^5+D_3 s^3+D_1 s} \tag{10}$$

where s is a complex variable, $N(s)$ and $D(s)$ are numerator and denominator respectively, and $N_4=\bar{M}^2\mu_m, N_2=-\mu_m\left(2\bar{M}\bar{K}-C_d{}^2\right), N_0=\bar{K}^2\mu_m,\ D_5=\left(\bar{M}^2\left(\mu_m^2+R_mR_r\right)+m^2e^2R_m\bar{C}\right),$
$D_3=-\left(\mu_m^2+R_mR_r\right)\left(2\bar{M}\bar{K}-C_d{}^2\right)$ and $D_1=\bar{K}^2\left(\mu_m^2+R_mR_r\right).$

The root-loci plot (*see* Fig. 10(a)) clearly shows how the closed loop poles vary with the system gain parameter i.e., supply voltage (V_s) in the complex *s*-plane. This diagram also confirms the existence of the Sommerfeld effect through the presence of multiple roots between the break-away marked as '*b'* and break-in marked as '*a'* point with gain parameter (V_s) 463 V and 168 V respectively for $i_0=0.6$ A and $\tau=0.001$ s. It is well-known from the linear control theory that the break-away (with maximum gain) and break-in (with minimum gain) can be obtained using the condition $(dV_s/ds=0)$. The points 'b'' and 'a'' in the root loci plot (as shown in Fig. 10 (a)) corresponds to the points '*b* 'and *'a'* respectively as shown in Fig. 10 (b) where the jumps are shown by the dash line during the coast up and coast down respectively.

4.2 Saddle-node bifurcation

Considering the bias current (i_0) as a bifurcation parameter with fixed time delay, the distance between the break-away and break-in point found to be reduced. Finally, these two points are found to be merged into a single point known as bifurcation point by annihilating each other when bias current (i_0) attains 4.598 A with the same time delay (*i.e.,* $\tau=0.001$) with supply voltage (V_s) is 437 V shown Fig. 11 (a). This kind of bifurcation is referred to as cyclic saddle node bifurcation [41]. The complete cessation of the Sommerfeld effect is observed when $i_0 >$ 4.598 A as shown in Fig. 11 (b).

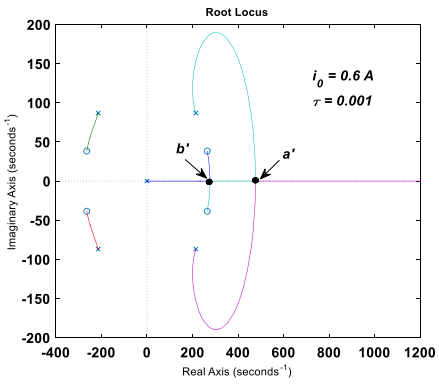

Fig. 10 (a) Root-locus plot of Eq. (10) for $i_0=0.6$ A and $\tau=0.001$

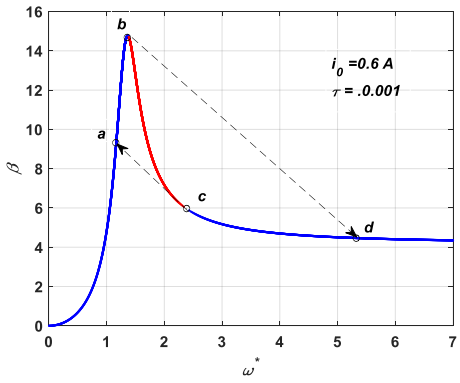

Fig. 10 (b) Nonlinear jumps in frequency response for $i_0=0.6$ A and $\tau=0.001$

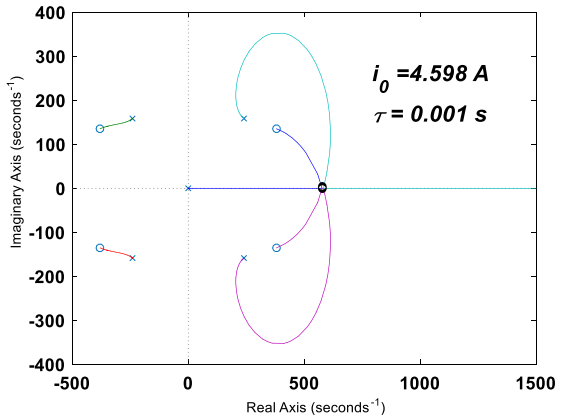

Fig. 11 (a) Root-locus plot of Eq. (10) for $i_0 = 4.598$ A and $\tau = 0.001$

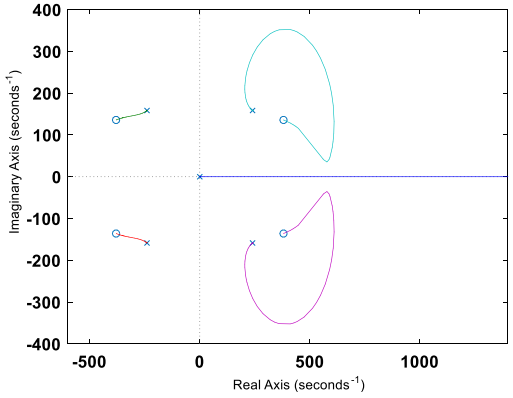

Fig. 11 (b) Root-locus plot of Eq. (10) for $i_0 > 4.598$ A and $\tau = 0.001$

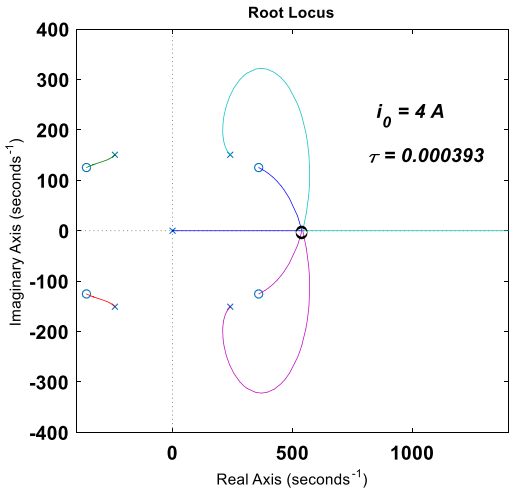

Fig. 12 (a) Saddle-node point for critical time delay $\tau_c = 0.000393$

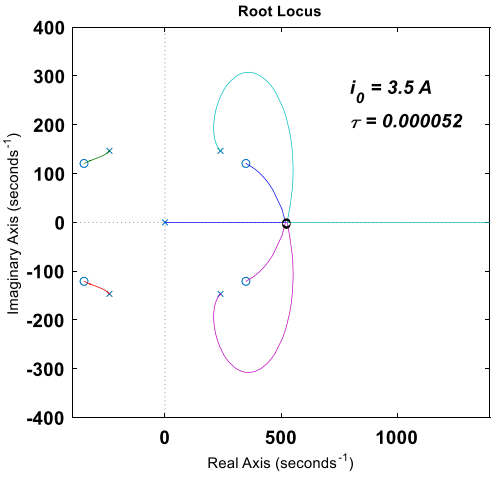

Fig. 12 (b) Saddle-node point for critical time delay $\tau_c = 0.000052$

On the other hand, considering the time delay as bifurcation parameter, the saddle node bifurcation occurs when time delay attains its critical value $\left(i.e., \tau_c = 0.000393\right)$ for fixed bias current shown in Fig.12 (a). The Sommerfeld effect would disappear completely when $\tau < 0.000393$. Fig.12 (b) illustrates the same phenomena for a much lower value of bias current, the saddle-node appears when the critical time delay is found to be much lower i.e., $\tau_c = 0.000052$. These critical values of time delays are negligibly small for a digitally controlled AMB system and not feasible. The above-mentioned numerical experimentation reveals that the saddle-node bifurcation is not practically achievable considering the time delay as a bifurcation parameter because the critical time delays are found to be negligibly small and hence not practicable for relatively smaller fixed bias current.

4.3. Hopf bifurcation

Using the transfer function given in Eq. (10) with supply voltage (V_s) as a gain parameter, the following fifth order polynomial can be constructed as:

$$F(s)=\sum_{i=0}^{5}a_i s^i = a_5 s^5 + a_4 s^4 + a_3 s^3 + a_2 s^2 + a_1 s + a_0 \tag{11}$$

where

$a_5=\left(\bar{M}^2\left(\mu_m^2+R_mR_r\right)+m^2e^2R_m\bar{C}\right)$, $a_4=V_s\bar{M}^2\mu_m$, $a_3=-\left(\mu_m^2+R_mR_r\right)\left(2\bar{M}\bar{K}-C_d{}^2\right)$, $a_2=-V_s\mu_m\left(2\bar{M}\bar{K}-C_d{}^2\right)$, $a_1=\bar{K}^2\left(\mu_m^2+R_mR_r\right)$ and $a_0=V_s\bar{K}^2\mu_m$.

According to the Routh-Hurwitz stability criteria [40], the vibratory response is stable if all nonzero a_i in Eq. (11) have the same positive or negative sign (necessary condition) and the corresponding all the Hurwitz determinants must be positive $(D_i, i=1,2,..,5)$ (sufficient condition) which implies,

$$D_1=a_4>0,\ D_2=\begin{vmatrix}a_4 & a_2\\ a_5 & a_3\end{vmatrix}>0, D_3=\begin{vmatrix}a_4 & a_2 & a_0\\ a_5 & a_3 & a_1\\ 0 & a_4 & a_2\end{vmatrix}>0, D_4=\begin{vmatrix}a_4 & a_2 & a_0 & 0\\ a_5 & a_3 & a_1 & 0\\ 0 & a_4 & a_2 & a_0\\ 0 & a_5 & a_3 & a_1\end{vmatrix}>0, D_5=\begin{vmatrix}a_4 & a_2 & a_0 & 0 & 0\\ a_5 & a_3 & a_1 & 0 & 0\\ 0 & a_4 & a_2 & a_0 & 0\\ 0 & a_5 & a_3 & a_1 & 0\\ 0 & 0 & a_4 & a_2 & a_0\end{vmatrix}>0.$$

As the time delay (τ) exceeds a critical value (τ_c), a pair of complex conjugate roots will cross the imaginary axis which leads to Hopf bifurcation with multiplicity of two. On substituting $s=j\omega$ in Eq. (11) and separating the real and imaginary parts leading to $\mathrm{Re}\left(F(j\omega)\right)=0$ & $\mathrm{Im}\left(F(s)\right)=0$. Now choosing the time delay (τ) as a bifurcation parameter, one may apply the transversality condition *i.e.,* $\mathrm{Re}\left(d\tau/ds\right)\big|_{\pm i\omega_0}>0$ for the occurrence of the Hopf bifurcation [23]. Using the above conditions for the occurrence of Hopf bifurcation, a set critical time delays (τ_c) may be obtained numerically for different fixed bias currents. In the root locus diagram as shown in Fig. 13 (a), the Hopf bifurcation is observed as two complex conjugate pairs are seen to cross the imaginary axis simultaneously when the time delay becomes 0.4361 for a fixed bias current 0.45 A. The corresponding phase plot as shown in Fig. 13(b) confirms the existence of Hopf as a typical wire framed paraboloid [42, 43] is formed. This paraboloid represents a limit cycle with time delay as a bifurcation parameter representing the third dimension. This unstable limit cycle confirms the presence of Hopf as the solution goes to infinity. A couple of similar kind of Hopf bifurcations may be obtained for different critical time delays as illustrated in Fig. 14 (a) and Fig. 14(b).

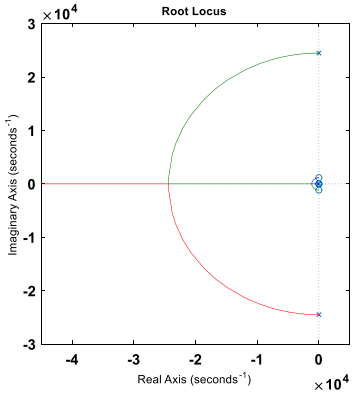

Fig. 13 (a) Root-loci plot when $\tau_c = 0.4361$ for $i_0 = 0.45$ A.

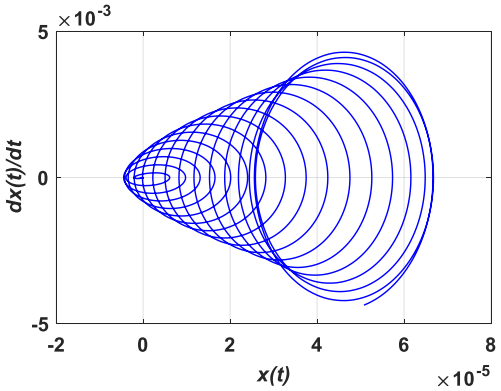

Fig. 13 (b) Phase-portrait when $\tau_c = 0.4361$ for $i_0 = 0.45$ A.

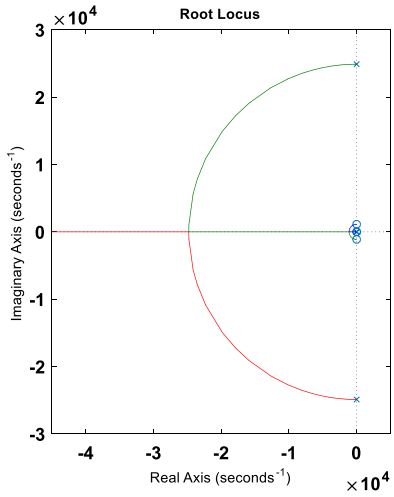

Fig. 14 (a) Root-loci plot when $\tau_c = 0.2991$for $i_0 = 0.64$ A.

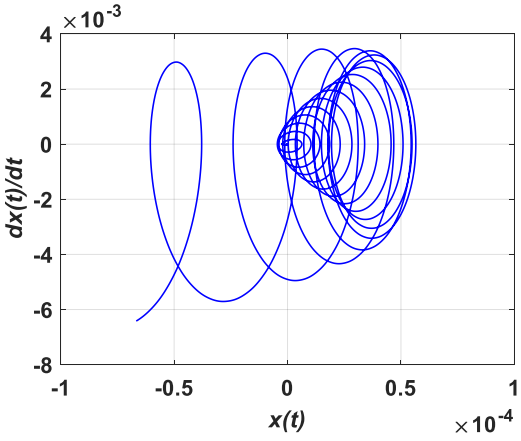

Fig. 14 (b) Phase-portrait when $\tau_c = 0.2991$ for $i_0 = 0.64$ A.

4.4 Trans-critical bifurcation

Another kind of bifurcation is observed through the root locus as shown in Fig. 15(a). A critical time delay $(\tau_c) =$ 0.002961 is obtained numerically with a given bias current $(i_0) = 1.2$ A for a certain condition, $C_d^2 > 4\bar{M}\bar{K}$. At critical value of the time delay, a discontinuous line is seen in the left portion of the frequency response curve as given in Fig.15 (b) which clearly a sign of inception of instability occurs at τ_c owing to the presence of a pair of complex conjugate poles with positive real parts lying on the right half plane of the root locus as shown in Fig. 15 (a). For $\tau < \tau_c$, the Sommerfeld effect is seen to be present in the form of jump phenomena where in near to the critical speed, the amplitude jumps to a lower value and the rotor speed jumps to a much higher value as shown Fig.16 (b) corresponds to a root locus plot shown in Fig.16 (a). A similar kind of jump is discussed in Fig.10 in which the break-in and break-away points are illustrated corresponding to minimum and maximum gain respectively. On the contrary, when $t > \tau_c$, the jump phenomena still exist but in the reverse manner *i.e.,* at the

very outset, the jump occurs leading to a discontinuous region marked in red color in the frequency response diagram as shown in Fig.17 (b) where the steady state solution does not exist and the value of damping is found to be negative causing self-excited vibration. The Fig. 17 (a) shows the root-locus diagram corresponds to Fig. 17 (b) also confirms the switching of stability as the nature of the root loci is just appeared in a reverse manner relative to Fig.16 (a). Owing to presence of negative damping at the beginning of run up, the rotor system attains its instability threshold at the very outset. Moreover, the break-in and break -away points are also found to be swapped with each other. This kind of switching of stability refers to as trans-critical bifurcation [44] as the corresponding break-in and break-away points will never destroy each other but switching the stability as the time delay (i.e., bifurcation parameter) becomes greater or lesser than its critical value (τ_c).

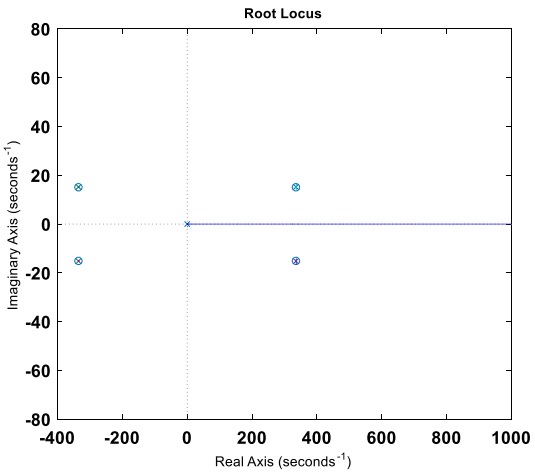

Fig.15 (a) Root-loci plot when $\tau_c = 0.002961$ for $i_0 = 1.2$ A.

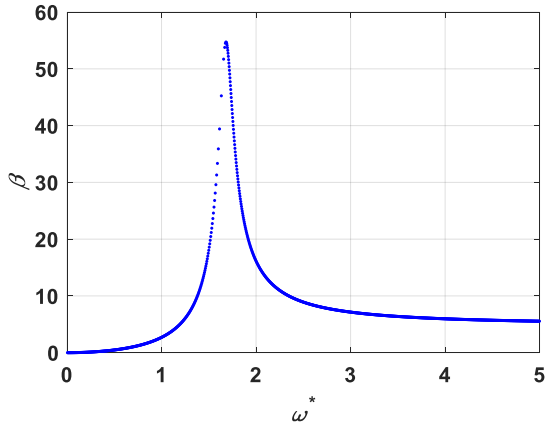

Fig. 15 (b) Frequency response diagram when $\tau_c = 0.002961$ for $i_0 = 1.2$ A.

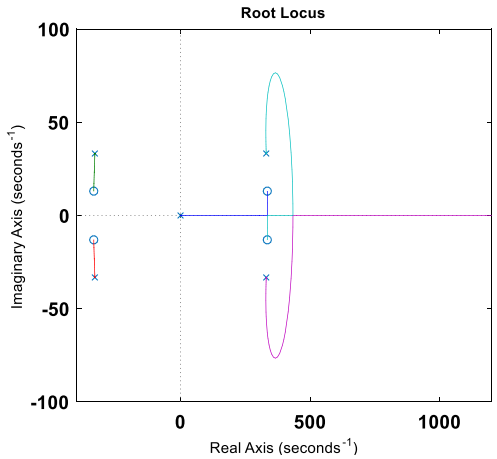

Fig. 16 (a) Root-loci plot when $\tau_c < 0.002961$ for $i_0 = 1.2$ A.

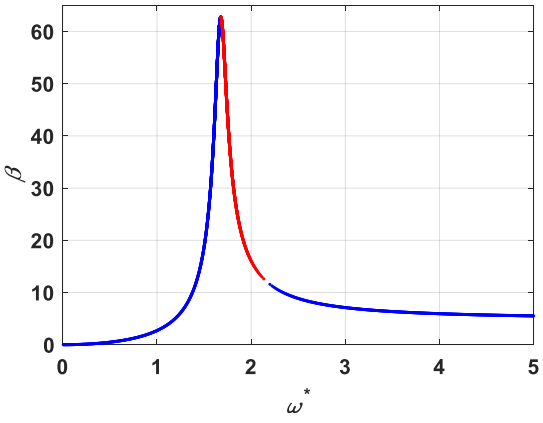

Fig.16 (b) Frequency response diagram when $\tau_c < 0.002961$ for $i_0 = 1.2$ A.

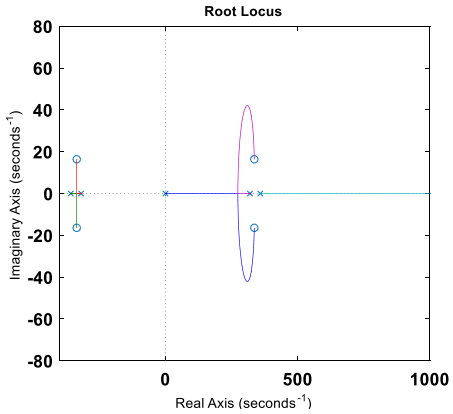

Fig. 17 (a) Root-loci plot when $\tau_c > 0.002961$ for $i_0 = 1.2$ A.

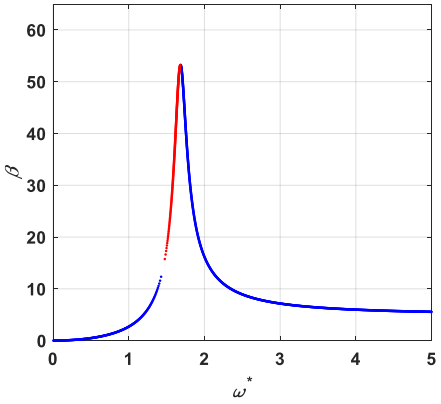

Fig. 17 (b) Frequency response diagram when $\tau_c > 0.002961$ for $i_0 = 1.2$ A.

5 Conclusion and future work

A novel approach is presented in this paper which reveals the influence of time delay on the complex dynamics of instability marked with nonlinear jumps exhibited by a non-ideal eccentric rotor with time-delayed AMB system. The analytical solution obtained through an energy balance confirms that the time delay indeed influences the attenuation of the Sommerfeld (*i.e.,* nonlinear jumps) effect with fixed bias current. It is evident from the frequency response diagram that the Sommerfeld effect starts attenuating as the time delay decreases. On fixing the time delay, the instability effect is also found to be attenuated as the bias current decreases. This observation reveals that the time-delayed AMB system is more economic compared to an AMB system without time delay aiming to suppress the Sommerfeld effect as in the latter case, the instability starts attenuating only when the bias current increases [21]. The transient analyses confirm the above-mentioned results obtained analytically. In addition, three different bifurcations are studied numerically using root-loci technique with time delay as a bifurcation parameter. The saddle node bifurcation occurs when the bias current attains a critical value for a given time delay at which the Sommerfeld effect is found to be disappeared completely. On the other hand, saddle-node also occurs at a specific critical time-delay with a given bias current. But the critical time delay is very small and hence not practicable for a digitally controlled AMB system. Following, Hopf bifurcation study reveals the existence of multiple Hopf points with the formation of a wire framed paraboloid in the phase-portrait which destabilizes the system further. Switching of stability is also observed at a critical time delay obtained with a specified condition. This switching of stability confirms the existence of trans-critical bifurcation. The present model of the rotor system with the inclusion of fractional order AMB with variable time delay along with the prediction of chaotic motion can be envisioned as a future work.

Compliance with ethical standards

Conflict of interest: The author declares no potential conflict of interest concerning the research, authorship, and/or publication of this article.

Data Availability Statements: Data sharing not applicable to this article as no datasets were generated or analysed during the current study.

References

1. Nayfeh, A.H., MOOK, D.T.: Nonlinear Oscillations. John Wiley & Son (1979)
2. Sommerfeld A: Beiträge zum dynamischen ausbauder festigkeitslehe. Phys Z. 3, 266–286 (1902)
3. Dasgupta, S.S.: Sommerfeld effect in internally damped shaft-rotor systems. (2011)
4. Felix, J.L.P., Balthazar, J.M., Brasil, R.M.L.R.F.: On tuned liquid column dampers mounted on a structural frame under a non-ideal excitation. J. Sound Vib. 282, 1285–1292 (2005). https://doi.org/10.1016/j.jsv.2004.05.006
5. Felix, J.L.P., Balthazar, J.M., Brasil, R.M.L.R.F., Pontes, B.R.: On Lugre Friction Model to Mitigate Nonideal Vibrations. J. Comput. Nonlinear Dyn. 4, 034503 (2009). https://doi.org/10.1115/1.3124783
6. Castaõ, K. Al, Goes, L.C.S.C.C.S., Balthazar, J.M.: A note on the attenuation of the sommerfeld effect of a non-ideal system taking into account a MR damper and the complete model of a DC motor. JVC/Journal Vib. Control. 17, 1112–1118 (2011). https://doi.org/10.1177/1077546310384000
7. Piccirillo, V., Tusset, A.M., Balthazar, J.M.: Dynamical Jump Attenuation in a Non-Ideal System Through a Magnetorheological Damper. J. Theor. Appl. Mech. 52, 595–604 (2014)
8. Kossoski, A., Tusset, A., Janzen, F.C., Rocha, R.T., Balthazar, J.M., Brasil, R.M.L.R.F., Nabarrete, A.: Jump attenuation in a non-ideal system using shape memory element. In: MATEC Web of Conferences (2018)
9. Jha, A.K., Dasgupta, S.S.: Suppression of Sommerfeld effect in a non-ideal discrete rotor system with fractional order external damping. Eur. J. Mech. A/Solids. 79, (2020). https://doi.org/10.1016/j.euromechsol.2019.103873
10. Jha, A.K., Dasgupta, S.S.: Sommerfeld Effect Attenuation Using Switched-Stiffness Method of a Non-ideal Internally Damped Shaft–Disk System with Constant Eccentricity. In: Lecture Notes in Mechanical Engineering. pp. 165–175 (2021)
11. Saeed, N.A., El-Ganaini, W.A.: Time-delayed control to suppress the nonlinear vibrations of a horizontally suspended Jeffcott-rotor system. Appl. Math. Model. 44, 523–539 (2017). https://doi.org/10.1016/j.apm.2017.02.019
12. Xuan, D.J., Kim, Y.B., Kim, J.W., Shen, Y.D.: Magnetic bearing application by time delay control. JVC/Journal Vib. Control. 15, 1307–1324 (2009). https://doi.org/10.1177/1077546308091460
13. Schweitzer, G., Maslen, E.H.: Magnetic bearings: Theory, design, and application to rotating machinery. (2009)
14. Eissa, M.H., Hegazy, U.H., Amer, Y.A.: Dynamic behavior of an AMB supported rotor subject to harmonic excitation. Appl. Math. Model. 32, 1370–1380 (2008). https://doi.org/10.1016/j.apm.2007.04.005
15. Tang, J., Xiang, B., Zhang, Y.: Dynamic characteristics of the rotor in a magnetically suspended control moment gyroscope with active magnetic bearing and passive magnetic bearing. ISA Trans. 53, 1357–1365 (2014). https://doi.org/10.1016/j.isatra.2014.03.009
16. Ghazavi, M.R., Sun, Q.: Bifurcation onset delay in magnetic bearing systems by time varying stiffness. Mech. Syst. Signal Process. 90, 97–109 (2017). https://doi.org/10.1016/j.ymssp.2016.12.016
17. Yoon, S.Y., Di, L., Lin, Z.: Unbalance compensation for AMB systems with input delay: An output regulation approach. Control Eng. Pract. 46, 166–175 (2016).

https://doi.org/10.1016/j.conengprac.2015.11.002
18. Yu, C., Sun, Y., Wang, H., Shi, F., Chen, Y., Shan, W.: Influence of conical degree on the performance of radial and axial integrated auxiliary bearing for active magnetic bearing system. J. Mech. Sci. Technol. 33, 4681–4687 (2019). https://doi.org/10.1007/s12206-019-0911-z
19. Su, W., Zheng, K., Liu, H., Yu, L.: Time delay effects on AMB systems. 2009 IEEE Int. Conf. Mechatronics Autom. ICMA 2009. 4682–4686 (2009). https://doi.org/10.1109/ICMA.2009.5244771
20. Eissa, M., Kamel, M., Al-Mandouh, A.: Vibration suppression of a time-varying stiffness AMB bearing to multi-parametric excitations via time delay controller. Nonlinear Dyn. 78, 2439–2457 (2014). https://doi.org/10.1007/s11071-014-1601-0
21. Jha, A.K., Dasgupta, S.S.: Attenuation of Sommerfeld effect in an internally damped eccentric shaft-disk system via active magnetic bearings. Meccanica. 54, 311–320 (2019). https://doi.org/10.1007/s11012-018-00936-7
22. Ji, J.C.: Dynamics of a Jeffcott rotor-magnetic bearing system with time delays. Int. J. Non. Linear. Mech. 38, 1387–1401 (2003). https://doi.org/10.1016/S0020-7462(02)00078-1
23. Ji, J.C., Hansen, C.H.: Hopf bifurcation of a magnetic bearing system with time delay. J. Vib. Acoust. Trans. ASME. 127, 362–369 (2005). https://doi.org/10.1115/1.1924644
24. Inoue, T., Ishida, Y.: Nonlinear forced oscillation in a magnetically levitated system: The effect of the time delay of the electromagnetic force. Nonlinear Dyn. 52, 103–113 (2008). https://doi.org/10.1007/s11071-007-9263-9
25. Eissa, M., Kandil, A., El-Ganaini, W.A., Kamel, M.: Analysis of a nonlinear magnetic levitation system vibrations controlled by a time-delayed proportional-derivative controller. Nonlinear Dyn. 2, 1217–1233 (2015). https://doi.org/10.1007/S11071-014-1738-X
26. Dantas, M.J.H., Balthazar, J.M.: On the appearance of a Hopf bifurcation in a non-ideal mechanical problem. Mech. Res. Commun. 30, 493–503 (2003). https://doi.org/10.1016/S0093-6413(03)00041-7
27. Guo, S., Wu, J.: Introduction to Functional Differential Equations. In: Applied Mathematical Sciences (Switzerland). pp. 41–60. Springer New York, New York (2013)
28. Feng, J., Zhu, W.Q., Liu, Z.H.: Stochastic optimal time-delay control of quasi-integrable Hamiltonian systems. Commun. Nonlinear Sci. Numer. Simul. 16, 2978–2984 (2011). https://doi.org/10.1016/j.cnsns.2010.11.020
29. Insperger, T., Editors, T.E.G.O.: Time Delay Systems: Theory, Numerics, Applications, and Experiments. (2017)
30. Genta, G.: Dynamics of Rotating Systems. Springer US, New York, NY (2005)
31. Genin, J.: Effect of nonlinear material damping on whirling shafts. Appl. Sci. Res. 15, 1–11 (1966). https://doi.org/10.1007/BF00411540
32. Yang, T., Cao, Q.: Delay-controlled primary and stochastic resonances of the SD oscillator with stiffness nonlinearities. Mech. Syst. Signal Process. 103, 216–235 (2018). https://doi.org/10.1016/j.ymssp.2017.10.002
33. Olver, P.: Equivalence, invariants and symmetry. Cambridge University Press, New York (1995)
34. Marsden, J.E., Ratiu, T.S.: Introduction to Mechanics and Symmetry. 17, (1999). https://doi.org/10.1007/978-0-387-21792-5

35. Bhattacharyya, R., Mukherjee, A., Samantaray, A.K.: Harmonic oscillations of non-conservative, asymmetric, two-degree-of-freedom systems. J. Sound Vib. 264, 973–980 (2003). https://doi.org/10.1016/S0022-460X(02)01540-7
36. Samantaray, A.K., Dasgupta, S.S., Bhattacharyya, R.: Sommerfeld effect in rotationally symmetric planar dynamical systems. Int. J. Eng. Sci. 48, 21–36 (2010). https://doi.org/10.1016/j.ijengsci.2009.06.005
37. Bou-Rabee, N.M., Marsden, J.E., Romero, L.A.: Tippe top inversion as a dissipation-induced instability. SIAM J. Appl. Dyn. Syst. 3, 352–377 (2004). https://doi.org/10.1137/030601351
38. Zukovic, M., Cveticanin, L.: Chaotic Responses in a Stable Duffing System of Non-ideal Type. J. Vib. Control. 13, 751–767 (2007). https://doi.org/10.1177/1077546307072542
39. Suherman, S.: Vibration Suppression of Rotating Shafts Passing Thorough Resonances by Switching Shaft Stiffness. J. Vib. Acoust. Trans. ASME. 120, 170–180 (1998). https://doi.org/10.1115/1.2893801
40. Ogata, K.: Modern control engineering. Prentice-Hall, Upper Saddle River, NJ (2010)
41. Belato D: Nao-linearidades no Eletro Peˆndulo Doctoral dissertation, (1998)
42. Nave, G.K., Nolan, P.J., Ross, S.D.: Trajectory-free approximation of phase space structures using the trajectory divergence rate. Nonlinear Dyn. 1, 685–702 (2019). https://doi.org/10.1007/s11071-019-04814-z
43. Uteshev, A., Kalmár-Nagy, T.: Measuring the criticality of a Hopf bifurcation. Nonlinear Dyn. 101, 2541–2549 (2020). https://doi.org/10.1007/s11071-020-05914-x
44. Strogatz, H.S.: Nonlinear Dynamics and Chaos With Applications to Physics, Biology, Chemistry, and Engineering. CRC Press (1994)